SALYUT-7 / KOSMOS-1686
Re-Entry Prediction Activities at ESOC

H. Klinkrad

Mission Analysis Section, ESA/ESOC
Darmstadt, FRG

Abstract

Salyut-7, a precursor of the present MIR space station, was launched by the USSR on 19-Apr-1982 (COSPAR notation: 82-033A). Following a series of crew visits (Sojus T-5 to T-14) and dockings with supply spacecraft (Progress 13 to 24), Salyut-7/Sojus T-14 were complemented by an unmanned Kosmos-1686 module spacecraft on 02-Oct-85. After the separation and return to earth of Sojus T-14 on 21-Nov-85, the Salyut-7/Kosmos-1686 configuration remained unchanged, with a total mass of 40,150 kg, and an overall length of about 26.0 m.

The Salyut-7/Kosmos-1686 complex was left mothballed at an altitude of 475 km in Aug-1986, from where is started its descent into the atmosphere which led to a re-entry above South America at 03:45 UTC on 07-Feb-1991.

The present report provides an overview of activities at ESA/ESOC during the follow-up of the Salyut-7/Kosmos-1686 decay, and of related co-operations with space agencies, research institutes, and national bodies within the ESA Member States, within the US and within the USSR.

1. Introduction

The Salyut space station program of the USSR started with the launch of Salyut-1 on 19-Apr-1971. This spacecraft as well as all successors of the Salyut programme were launched by a 4-stage Proton D-1, with a lift-off mass of about 1,000 t and a maximum payload to LEO of 17 to 19 t (Salyut mass at launch: 18,900 kg). As of Salyut-6, the orbital laboratories were equipped with docking ports at both ends of the cylindrical body which could accommodate manned spacecraft of the Sojus series and unmanned supply spacecraft of the Progress type (with a mass of 7,000 kg, nearly 30% of which could be payload, including up to 1,000 kg of fuel).

The first generation of Salyut modules terminated with the end of service of Salyut-5. Maximum mission durations up to then were on the order of 2 years. The second generation of USSR space stations started with the lift off of Salyut-6 on 29-Sep-77. From then on, mission durations were increased by a factor 2, and scientific return was improved accordingly. Salyut-6 was also the first of the series to dock with a prototype of future space station modules (Kosmos-1267) on 25-Apr-81.

Salyut-7, launched on 19-Apr-82 (COSPAR designator: 82-033 A), was the sixth successful (Salyut-2 failed and decayed) and also the last of the Salyut space stations. Salyut-7 was visited by 10 Sojus spacecraft carrying 21 cosmonauts (one of them the French cosmonaut Jean-Loup Chretien), by 13 Progress supply ships, and by two large supply modules (Kosmos-1443 and Kosmos-1686) which could carry up to 6.5 t payload. The latter of these modules, which was of similar size and mass as Salyut-7, remained attached until re-entry (see Fig.1).

In Aug-1983 Salyut-7 received damage in its propellant supply system during re-fueling from Progress-17. While this malfunction was later resolved during 6 EVAs within 1984, western analysts observed that the Salyut-7 propulsion system has never been used since. Also in 1983, impact craters (most likely from orbital debris) were detected on one of the station viewports, and nearly resulted in an early mission abort.

After the orbital complex was mothballed by the crew of Sojus T-15 in May-1986, the engines of Kosmos-1686 were used to raise the orbit by some 135 km to a mean altitude of 475 km in order to counteract increasing airdrag with the approach of the maximum of solar cycle 23. At this point, Salyut-7/Kosmos-1686 had a total mass of 40,150 kg. Due to its shape and moments of inertia the complex acquired a gravity gradient passive stabilisation, with the longitudinal axis aligned with the geocentric radial. The offset between centre on mass and centre of aerodynamic pressure exerted a perturbing torque which resulted in a coning motion about the stable direction at a half cone angle of 10 to 20 deg.

The last communication with Salyut-7 was recorded in Dec-1989. Thereafter, the space station was expected to be no longer controllable (see, however, 3.3). By 15-Feb-1989, it had already decayed to a mean altitude of 415 km.

The Salyut-7/Kosmos-1686 compound was the largest space object to re-enter into the earth atmosphere since Skylab decayed on 11-Jul-1979. While Skylab with 74,250 kg had about twice the mass of Salyut-7, its orbit shape, altitude, and inclination were very similar. Likewise, the experience from Skylab concerning debris reaching the ground could be used as an indication for the estimation of debris dispersion signatures and residual on-ground risks.

Proc. Internat. Workshop on Salyut-7 / Kosmos-1686 Reentry, ESOC, Darmstadt (D), 9 April 1991

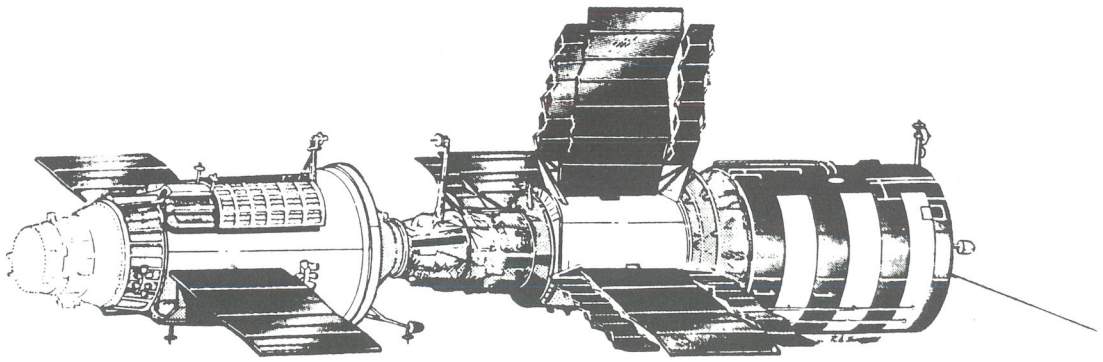

Figure 1. Re-Entry Configuration of Salyut-7/Kosmos-1686: This configuration (with Kosmos-1686 shown towards the left) remained unchanged since May 1986 when the station was mothballed. (Linedrawing courtesy of Teledyne Brown Eng.).

2. Organisation of the Campaign

The Mission Analysis Section of ESA/ESOC is coordinating activities of ESA establishments in the field of space debris, and is actively involved in all work related to the space debris environment, and aspects of orbit dynamics of the debris population. The latter task includes the identification of potential re-entry risk objects, the prediction of re-entry time windows and of associated ground-trace swath areas.

2.1 Sources of Information

After the abandoning of Salyut-7/Kosmos-1686 in Aug-1986, the complex was known to decay within a few years. ESOC started its re-entry prediction activities on a low scale in Jan-1990, predicting a decay by the end of Dec-1990. At this time, ESOC was receiving Two-Line Orbital Elements (TLEs) from USSpaceCom via NASA/JSC at a rate of one per week. These data contained the object identifier (COSPAR number 82-033A for Salyut-7, and 85-086A for Kosmos-1686), epoch of ascending node close to time of orbit determination, mean orbital elements (Kepler elements, with mean motion n instead of semimajor axis, compatible with the SGP-4 orbit theory of USSpaceCom) and ballistic parameter information (in terms of $\dot{n}/2$, $\ddot{n}/6$ and $B^{\times}$, the latter one being specific for the SGP-4 orbit theory).

In Nov-1990, following an agreement with NASA/JSC, the transmission rate of Salyut-7/Kosmos-1686 TLEs (also known as ELSETs in the US) was increased to 3 per week. This corresponds to the rate at which NASA/GSFC is receiving the information from USSpaceCom via magnetic tape. The TLE information was forwarded from GSFC to JSC and transmitted to ESOC as MAIL to the ESOC communication node ECD1 (a VAX 3800, also known as NSP = Network Systems Processor) via SPAN (the Space Physics Analysis Network).

As of Nov-1990, supplementary TLE sets were also sent to ESOC directly from GSFC via Telefax. The initial transmission rate was less that for the JSC SPAN data, however, as the re-entry date approached, the GSFC information came in at steadily increasing rates, covering up to 30% of all ascending node states on the last day before decay. By this time, GSFC became the most responsive data source from the US, with time lags between orbit determination and TLE reception at ESOC as short as 2 orbital revolutions (3 hours and less).

The GSFC orbital data on Salyut-7/Kosmos-1686 were complemented by TLE sets which were received at ESOC via Telefax from RAE Farnborough during the last week of the orbital lifetime. While this information was basically redundant with the GSFC data, in many cases the response time was again decreased, due to the geographical proximity of the Fylingdales radar from where the data were forwarded.

As a result of an initiative taken by the director of FGAN (Research Establishment for Applied Science, Wachtberg-Werthhoven/FRG) and the director of ESA/ESOC, FGAN favourably responded to ESOC's request for support, and shared tracking data (range, range-rate, and angular measurements) and derived TLEs with ESOC. This source of information for the first time allowed the processing of data other than from USSpaceCom (see also 2.2). The FGAN data were transmitted to the ESOC communication node (NSP) via the DATEX-P public network. As for all E-mail data, the files were routed from the NSP (VAX 3800) to the operational Comparex/MVS mainframe, were the tracking data were used for orbit determination, and then translated into TLE format before the state vectors were merged with the FGAN TLE results and external TLE information.

The FGAN radar is the most powerful and efficient installation outside the USSpaceCom surveillance network in Europe. Its 34 m dish antenna allows tracking operations in L-Band, and imaging in Ku-Band with high efficiency. As of mid Jan-1991, FGAN was tracking Salyut-7/Kosmos-1686 and transmitting the data to ESOC once per week. Regular phone links between ESOC and FGAN also provided recent analysis results

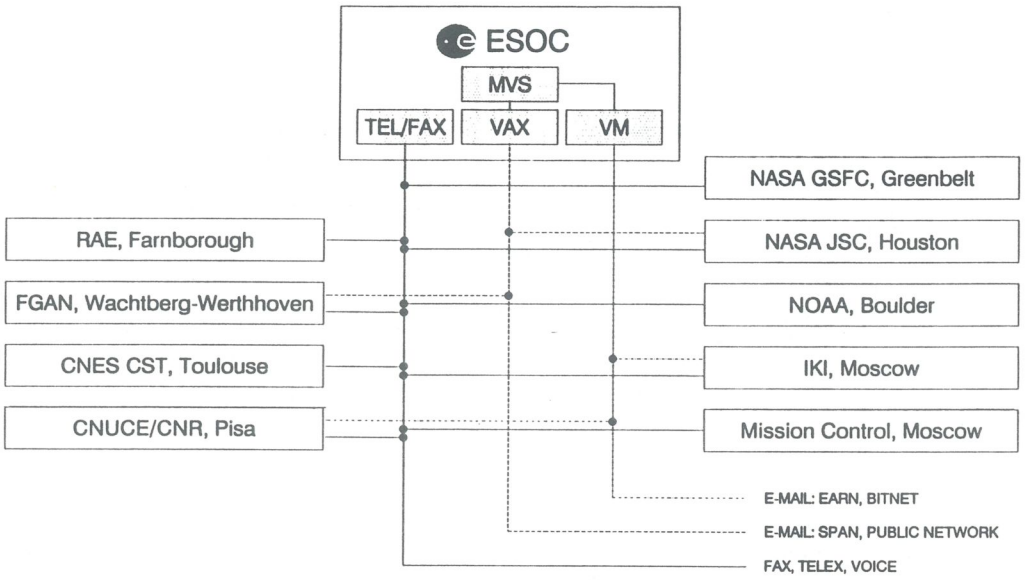

Figure 2. ESOC Communication Links for the Salyut-7/Kosmos-1686 Re-entry: All computations were performed on a Comparex (MVS) mainframe, while data were received through the ESOC PROFS machine (VM), the VAX communication node (NSP machine), and via FAX hardcopies.

of FGAN experts on the attitude of the object from the interpretation of radar images in Ku-Band. During the last week before re-entry, the data transmission rate from FGAN to ESOC was increased to cover all of the 4 to 5 passes seen by the radar each day.

Following a request for support to the Director of the TSUP Mission Control Centre (Kaliningrad), and to the Director of IKI (the Institute for Cosmic Research, Moscow), ESOC received regular orbit determination results from the USSR authorities as of the end of Jan-1991. Towards re-entry, the transmissions (which came via Telefax on a reserved line) were received within 1 hour of the orbit determination. Since FGAN could not observe the last 16 hrs of Salyut's lifetime (the re-entry was 20 min short of the next FGAN acquisition), the data from the USSR came in fastest at ESOC during the last day.

Additional information on lifetime prediction and orbit determination of Salyut-7/Kosmos-1686 was received by Fax and E-Mail (EARN/BITNET) from CNES/CST (Toulouse/F), and from CNUCE/CNR (Pisa/I). Re-entry predictions, supplementing the orbital data, were also send via Fax from GSFC (TIPs = Trajectory & Impact Predictions), IKI (routing information also for the Ministry of Defence and the MCC), and RAE Farnborough.

In addition to orbit and attitude information, the solar and geomagnetic activities which primarily drive the upper atmosphere density are of paramount importance for the deduction of the ballistic parameter of the spacecraft, and for the prediction of the remaining orbital lifetime.

ESOC regularly acquires data on solar activity (in terms of $F_{10.7}$, the 10.7-cm radio flux of the day in question in units of 10^4 Jansky, and $\bar{F}_{10.7}$, a 90-day running mean value), and of geomagnetic activities (in terms of the daily planetary amplitude index A_p). These data are received on the NSP VAX (via SPAN) from the Level B Datacentre at Edinburg/UK, and transferred to the operational Comparex/MVS computer where a file with daily records is maintained. The data received on day t contain solar activity data of day $t - 1d$, and finalised geomagnetic activity indices of day $t - 2d$. Preliminary A_p values are also indicated for day $t - 1d$, and short-term forecasts are given for all activity numbers up to day $t + 2d$.

Fig.2 summarises the data flow to ESOC from NASA GSFC (TLEs and TIP re-entry predictions), NASA JSC (TLEs), FGAN (TLEs, tracking data, attitude information, and re-entry forecasts), RAE (TLEs and re-entry predictions), IKI/MCC (orbit states and re-entry predictions), NOAA (solar and geomagnetic activity measurements and forecasts), CNUCE and CNES (re-entry predictions).

As an alternative to the E-mail data transfer, ESOC receives Telexes with SOLTERWARN Bulletins via FTZ (the Telecommunication Technology Centre of the German PTT at Darmstadt).

2.2 Processing of Information

For long-term orbit predictions, the modelling of solar and geomagnetic activity evolutions with time is essential (see history in Fig.4). For this purpose ESOC/OAD have established a forecasting software tool under contract with the University of Edinburg/UK (Ref.8). Based on previous solar cycle histories and on histories of monthly means, the software predicts monthly means of $\bar{F}_{10.7}$ and A_p by the McNish-Lincoln method (which is also employed by MSFC Atmospheric Sciences Div. for their predictions issued under code ES84). The activity forecasts include $+1\sigma$ uncertainty levels and take into account mean monthly history records for a prediction period of about 12 months. Thereafter, the prediction process reverts to the reproduction of a mean solar cycle with mean cycle length.

For A_p forecasts, only the part which correlates with the solar cycle can be reproduced. This prediction, however, can be exceeded by a factor 10 or more in case of geomagnetic storms.

Solar and geomagnetic activity data are the only non-deterministic model parameters for the determination of air density at thermospheric altitudes. All other density parameters (longitude, latitude, LST, UT, altitude, and day of the year) can be determined from a given orbit state at epoch. Likewise, the state at epoch unambiguously defines the perturbation environment due to potential forces (geopotential harmonics, and lunisolar perturbations). For a given area-to-mass ratio A/m of a spacecraft, also the major non-conservative perturbations airdrag and solar radiation pressure can be modelled, provided that a corresponding drag coefficient c_D and reflectivity coefficient c_R is given or calibrated with observations via an orbit determination process (see 3.4 and 3.6).

Having formulated an adequate perturbation model, a state vector at epoch is necessary which is compatible with the perturbation model formulation, and with the orbit propagation technique used (see 3. and 4. for details). The ESOC re-entry prediction software uses two different sets of orbital elements:

- singly averaged mean Kepler elements (averaged with respect to M according to Liu and Alford, Ref.7); used for long-term orbit prediction (a few days to a few years) with large step sizes (from 2 down to 0.1 days)
- osculating Kepler elements used for final re-entry prediction (downwards from 170 km altitude) with small step sizes (1/80 to 1/200 of the nodal period)

All orbit propagation is performed in a mean-of-date equatorial coordinate system, with UTC time scale, and time encoded as Modified Julian Date 1950.0 (MJD1950.0).

Different data sources provided ESOC with orbit state information at epoch in different formats:

- TLE Data Format: used by NASA GSFC, NASA JSC, RAE Farnborough, FGAN; providing a mean Kepler state vector (according to SGP-4 theory), with mean nodal frequency (in rev's/day) instead of semimajor axis; time is in UTC and encoded as YYDDD.DDDDDDDD for epochs of ascending node crossings (except for FGAN); the coordinate frame is a true-of-date system with mean equinox
- USSR Data Format: used by Department of Defence, TSUP, and IKI; providing osculating Kepler elements, with nodal period instead of semimajor axis; time is given as UTC in date format YYMMDD HHMMSS.SSSS for epochs of ascending node crossings; the coordinate frame is a mean-of-date system of 1950.0

The ESOC orbit determination results from FGAN tracking data were generated as osculating elements, compatible with the numerical final re-entry prediction software.

Before further processing, the USSR data were converted to osculating Kepler elements by iteratively solving the following implicit expression of $a = a(T_N, i, e, \omega)$ given by Blitzer in terms of osculating elements at ascending node (Ref.2).

$$T_N = 2\pi \sqrt{\frac{a^3}{\mu}} \left[1 - \frac{3J_2(1 + e\cos\omega)^3}{2(a/a_e)^2(1-e^2)^3} - \frac{3J_2(4 - 5\sin^2 i)}{4(a/a_e)^2\sqrt{1-e^2}\,(1+e\cos\omega)^2} \right] \quad (1)$$

where $a_e = 6378.135$ m is the earth's normalising equatorial radius, and T_N is the nodal period.

In order to translate the different orbit and epoch data into the format(s) required by the ESOC software, a tool is used (called CSTATE) which allows orbit state and epoch conversion to and from any of the following alternative formulations:

- Time Scale Options: TAI (International Atomic Time), UTC (Universal Time Coordinated), ET (Ephemeris Time)
- Epoch Format Options: Modified Julian Date 1950.0 (MJD 1950.0), Modified Julian Date 2000.0 (MJD 2000.0), Date Format (YY/MM/DD HH/MM/SS.SSSS), TLE Date Format (YY/DDD.DDDDDDDD)
- Coordinate Frame Options: Mean System of 1950.0, Mean System of 2000.0, Mean System of Date, True System of Date
- Analytical Orbit Theory Options: None (osculating state), SGP Theory (based on Kozai, doubly averaged), SGP-4/SDP-4 Theory (based on Brouwer, doubly averaged), SGP-8/SDP-8 Theory (based on Brouwer, doubly averaged), Liu Theory (based on Liu and Alford, singly averaged), Aeronutronic Theory (based on Brouwer, doubly averaged, similar to SGP-4)
- Orbit State Options: Cartesian State Vector, Kepler State Vector (with a, e or n, e or h_{pe}, h_{ap}), Equinoctial State Vector (non-singular for $e \to 0$ or for $e, i \to 0$)
- Fast Angular Variable Options: Mean Anomaly, True Anomaly, Eccentric Anomaly

2.3 Distribution of Results

Based on the input data described above, ESOC performed orbital lifetime and re-entry predictions for the Salyut-7/Kosmos-1686 spacecraft complex (see 3. and 4. for details of the methods). As of 03-Dec-90, a total number of 11 Re-Entry Prediction Bulletins were issued, providing background information and updates of the predicted re-entry date. As the re-entry came closer, the Bulletins contained prediction results with increasing information content including: centre of impact window (COIW, epoch and geographic position), width of re-entry time window (centred on COIW), current mean altitude, mean decay rate, and nodal period. Early releases of the Bulletin showed a world map, indicating the endangered latitude bandwidth ($\pm$ 51.7°). The last issues had three maps attached:

- World Map (see Fig.5): showing the potential groundtracks over 1 day or over the re-entry time window (whichever is smaller), centred on the time of COIW; the groundtracks were generated with a drag-free analytical orbit theory using an interme-

diate state from the time of transition of a mean altitude of 170 km; relative orbit numbers (counted backward and forward from the most likely re-entry orbit, centred on COIW) and epochs of ascending and descending node passes were indicated (example: -1/02:38, denoting 1 orbit before most likely re-entry orbit, passing the indicated point near the node at 2:38' UTC).

- Map of Europe: showing a close-up of Europe, with political boundaries and major cities; providing groundtracks with labels in 2-minute intervals which contain relative orbit number and epoch (same format as before).
- Map of Canada: showing a close-up of Canada and parts of the US (same features as for Europe Map)
- Headers: All maps are given with a 4-line header which is automatically composed from different input and output files of the re-entry prediction run; the header contains the COSPAR identifiers, the epoch from where the prediction was started, and the computed time and location of the COIW

During the final 12 hrs of the orbital lifetime of Salyut-7/Kosmos-1686, the production of Re-Entry Prediction Bulletins was discontinued (after issue no.11), and shorter Information Notes were prepared (6 in total). These concentrated on updates of COIW time and location, and on re-entry time window updates, including supporting maps.

ESOC distributed re-entry prediction information in form of Bulletins or Information Notes via FAX, and also provided intermediate information via voice links. The national points of contact within the ESA Member States and Associated Member States were: the Austrian Space Agency (A), Ministere de l'Interieur (B), Canadian Space Agency (CDN), Danish Civil Defence and Emergency Planning Agency (DK), CNES (F), BMI (D), DLR (D), Irish Science and Technology Agency (IRL), Ministero dell' Universita e della Ricerca Scientifica e Tecnologica (I), Ministry for Internal Affairs (NL), Ministerio del Interior (E), Swedish Space Corporation (S), Swedish National Space Board (S), Nationale Alarmzentrale (CH), Federal Office for Education and Science (CH), and the British National Space Council (UK).

Further technical information exchange (via voice links, FAX or E-mail) took place between ESOC and the following Technical Points of Contact: FGAN/FHP (D), DLR (D), CNES (F), CNUCE/CNR (I), RAE (UK), NASA/GSFC (USA), NASA/JSC (USA), and IKI (USSR) (see Fig.2).

3. Long-Term Re-Entry Prediction

3.1 Semi-Analytical Prediction Method

The long-term orbit prediction for Salyut-7/Kosmos-1686 was performed by means of a semi-analytical technique which propagates singly averaged orbital elements (J_2 first order means according to Liu and Alford) by numerical integration of averaged (over the mean anomaly M) perturbation equations. The method assumes a frozen perturbation environment over the averaging interval (the anomalistic period at epoch), performs a separation of perturbations for the averaging operation, superimposes the resulting mean time rates of change of the Kepler orbital elements, and forwards the lumped right hand sides of the perturbation equations to the integrator.

The integration of the averaged, perturbed equations of motion is performed by a multi-step Adams-Bashforth/Adams-Moulton predictor/corrector algorithm of user definable order (between 1 and 8), and fixed step size. The starting arc for the integration is established by a single-step Runge-Kutta/Shanks 7/8 method. As a good compromise with regard to accuracy and numerical stability, a 4-th order integrator with 1 corrector step was used throughout the computations. The integration step sizes were initially (3 months before decay) set at 1 day, and reduced to less than 0.25 days during the last month of the orbital lifetime.

The long-term prediction technique is implemented in a program called FOCUS (Fast Orbit Computation Utility S/W). It allows to take into account the following perturbations:

- geopotential: with harmonics up to degree and order 23, including $(J_2)^2$ second order terms; according to Kaula (Ref.5)
- airdrag: with air densities according to MSIS-77 or MSIS-86 (CIRA-86); including diurnal bulge, corotating atmosphere, and harmonic satellite cross-section variation (e.g. sun-pointing solar arrays); according to Klinkrad (Ref.6)
- luni-solar third body: with expansions of the perturbation functions up to degree and order 23; according to Cook (Ref.3)
- solar radiation pressure: including eclipses for spherical or oblate earth; assuming a constant effective cross-section (e.g. sun-pointing solar arrays); according to Aksnes (Ref.1)

All perturbations are averaged independently (separation of perturbations) in a purely analytical, closed-form manner in order to determine the individual contributions to the total mean time rates of change of the Kepler state vector elements. In all cases the averaging operation is performed over an arc of 2π of the mean anomaly M (one anomalistic revolution). In case of airdrag and radiation pressure, however, the eccentric anomaly E is used as integration variable, employing the transformation relation

$$dM = \frac{r}{a}\, dE = (1 - e \cos E)\, dE \qquad (2)$$

For re-entry predictions to ground, the semi-analytical FOCUS program stops the integration at a user defined threshold altitude ($h = 170$ km was selected) which marks the limit of validity of the simplifying perturbation model assumptions (e.g. airdrag is no longer a second order perturbation). At this point, the final mean Kepler state vector is converted to a 1-st order (J_2) osculating Kepler state (according to Liu and Alford, Ref.7) and written to a file together with all model parameter values and option settings. This file is thereafter read by the numerical integrator (see 4.) which propagates the state deep into the atmosphere ($<$ 30 km altitude) to mark the COIW time and location.

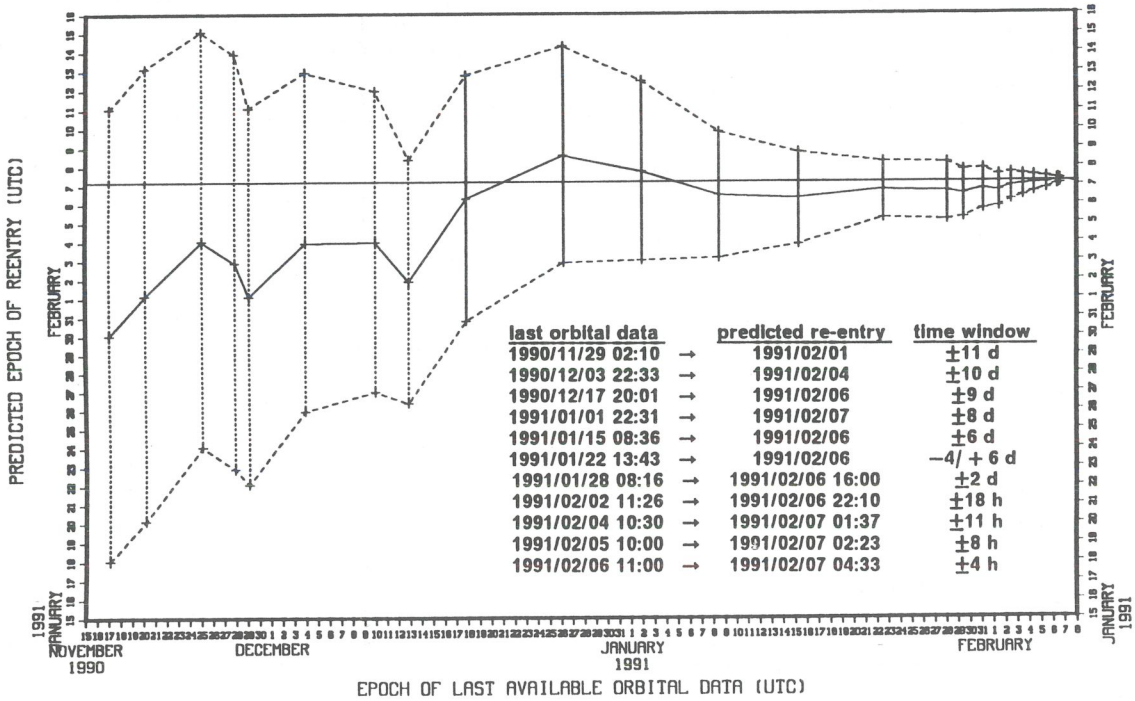

Figure 3. Salyut-7/Kosmos-1686 Re-Entry Prediction History: Solid line = nominal centre of impact window (COIW) prediction, dashed lines = width of expected re-entry time window, Vertical bars = markers for epochs when predictions were performed. The insert shows a summary of re-entry forecasts from Prediction Bulletins No.1-11.

3.2 Initial Orbit State

The program FOCUS performs its computations in terms of singly averaged Kepler elements according to Liu and Alford (Ref.7), with UTC time scale (time encoded as MJD 1950.0), and in a mean equatorial system of date. All input data are converted into this format before they enter the preprocessing (e.g. ballistic parameter fitting, and data analysis) and the orbit prediction modules.

The Kepler state and epoch used to start the orbit lifetime and re-entry prediction are taken without modification as provided by the data source and as converted by the CSTATE routine. Hence, no smoothing or RMS fitting of the state with respect to a preceding state history is performed. The program operator can, however, analyse a batch of state input records with regard to continuity and smoothness of the time history $a(t)$ of the semimajor axis. For this purpose, three options are available:

1. Least Squares Polynomial Fit $\tilde{a}(t)$: the time history $a(t)$ of the semimajor axis is fitted, without consideration of orbit mechanics; in the early phase of the orbit decay a polynomial of order 1 or order 2 (linear and quadratic terms in t) is normally adequate, whereas close to re-entry order 3 is recommended

2. Shooting Method by c_D Iteration: by backward orbit propagation to a target epoch t_{-k}, and by adaptation of the drag coefficient c_D via the regula falsi; the offset between predicted and observed $a(t_{-k})$ is successively reduced until a user defined threshold is met; the intermediate history $a(t)$ for $t \in [t_0, t_{-k}]$ properly reflects the orbit dynamics (in contrast with the $\tilde{a}(t)$ fit), and in particular considers the temporal variation in the airdrag environment (solar and geomagnetic activity)

3. Least Squares Fit $\hat{a}(t)$ by c_D Iteration: the same technique is applied as for the Shooting Method, however, all intermediate data points $a(t_{-i})$, $0 \le i \le k$ are taken into account, and c_D is adapted such that the total RMS deviation becomes a minimum; as for the Shooting Method (and in contrast with the Polynomial Fit), the initial condition $a(t_0)$ remains unchanged

The different techniques of $a(t)$ data analysis are given here in ascending order of CPU time consumption. Hence, for a quick-look data browse the Polynomial Fit should be preferred (see also 5.1).

3.3 Spacecraft Attitute

The Salyut-7/Kosmos-1686 station configuration (Fig.1), due to its elongated shape and corresponding moments of inertia, went into a gravity-gradient stabilisation (with Kosmos-1686 towards the earth) after it was mothballed in 1986. A priori analysis of perturbing torques indicated a stable coning motion around the radial, geocentric direction at a half-cone angle of approximately 10°. Observations by their imaging Ku-Band radar and analysis of the data by FGAN three months prior to decay confirmed a long-periodic coning motion at an opening angle of some 20° about the radial direction, with some

superimposed rotational motion of the S/C about its longitudinal axis (of poorly defined period).

The gravity gradient stabilisation was degrading strongly between two successive FGAN observations on Jan.17 and Jan.21, 1991. Thereafter, the complex started a rotation about its transverse axis at a steadily increasing rate. The rotation about the longitudinal axis was maintained at the same time.

On Feb.05 the Salyut-7/Kosmos-1686 compound was telecommanded into a head-on attitude (longitudinal axis aligned with the velocity vector) of minimum aerodynamic drag (note that the complex was deemed uncontrollable up to then). This alignment could be maintained for about 3 orbits, until excessive perturbing torques moved the S/C back into its preceding passive attitude mode. The head-on attitude was originally planned to be kept over 13 to 14 revolutions, in order to shift the re-entry orbit away from Europe to a longitude of the ascending node which entails a minimum on ground risk. Early fuel depletion, however, did not allow a successful completion of this manoeuvre.

3.4 Spacecraft Configuration

Information on the spacecraft mass m and normalising cross-section A is essential in order to establish a meaningful estimate of the drag coefficient c_D, and thus determine the ballistic parameter

$$B = c_D \frac{A}{m} \tag{4}$$

From the open literature the mass of the Salyut-7/Kosmos-1686 complex is given as about 20,000 kg (with 50% each for Salyut-7 and Kosmos-1686). For the forthcoming analysis, $m = 20{,}150$ kg shall be adopted, which is consistent with the source of the following geometric data.

Due to the predominantly gravity gradient stabilised attitude, the normalising cross-section of the S/C complex shall be based on the projection perpendicular to the longitudinal body axis. Based on detailed geometry information from FGAN, the minimum and maximum longitudinal cross-section was computed as $A_{min} = 100.1$ m² and $A_{max} = 152.6$ m². These values take into account the following contributions:

- minimum longitudinal cross-section A_{min} : body cross-section of 80.1 m², plus cross-section of one asymmetric Salyut-7 solar array of 20.0 m²
- maximum longitudinal cross-section A_{max} : body cross-section of 72.6 m², plus cross-section of four co-planar Salyut-7/Kosmos-1686 solar arrays of 80.0 m² (all arrays are of the same size)

The drag contribution from planar solar arrays over one orbit is proportional to $\sin \Psi$ and to $\sin |U + v|$, where Ψ, U, and v is the angle between the orbit normal and the sun direction, the argument of eccentric latitude, and a phase angle $v(\Omega, \omega)$. Hence, the locally effective aerodynamic cross-section is

$$A(U) = A_{min} + (A_{max} - A_{min}) \sin \Psi \sin |U + v| \tag{5}$$

averaging of $A(U)$ with respect to U leads to a mean aerodynamic cross-section of

$$\bar{A} = A_{min} + (A_{max} - A_{min}) \frac{2}{\pi} \sin \Psi \tag{6}$$

The corresponding area for Salyut-7/Kosmos-1686 was adopted as $\bar{A} = 126.4$ m². The validity of the resulting mean surface load of $m/\bar{A} = 159.4$ kg / m² is confirmed by realistic results of the calibrated c_D in section 3.6 .

3.5 Perturbation Environment Models

For the determination of the time rates of change of the mean orbital elements a precise formulation of analytically tractable perturbation functions is essential. The following models were used for the formulation of the main perturbing forces:

- Ephemerides: analytical expressions for the geocentric positions of sun and moon as a function of MJD1950.0; accuracies retained: better than 0.02° and 0.1°, respectively
- Reference Earth Ellipsoid: equatorial mean radius $a_e = 6378.144$ km, and earth flattening $f_e = 1/298.257$ (GEM-6 model)
- Solar & Geomagnetic Activities: observations and 3-day forecasts of $F_{10.7}$, $\bar{F}_{10.7}$ and A_p from NOAA/Boulder, on a file with daily entries; long-term forecasts, including 1-σ uncertainty levels for $\bar{F}_{10.7} = F_{10.7}$ and A_p from ESOC prediction S/W, based on a theory of McNish-Lincoln, contained in a file with monthly entries; the activity data are assumed centred on the day and month, respectively, with intermediate results obtained by linear interpolation in time
- Atmosphere Model (Air Density): MSIS-86 model, with density ρ as a function of geodetic altitude h, geodetic latitude ϕ, geographic longitude λ, local solar time τ, day of the year t_d, Universal Time (UT), a running 90-day mean $\bar{F}_{10.7}$ and current value $F_{10.7}$ (on previous day) of solar activity, and the planetary geomagnetic index A_p; for the averaging operations, UT/longitude density variations were disabled; for altitudes below 90 km the static US Standard Atmosphere 1976 was used; for altitudes in the homosphere-thermosphere transition, where 90 km $\leq h \leq$ 120 km, a fairing between MSIS-86 and USSA-76 was performed (see 4.2)
- Geopotential Model: GEM-10B model limited to degree 7 and order 0 (zonal harmonics J_2 to J_7)
- Luni-Solar Perturbation Model: perturbation function expansions up to degree and order 2 and 3 for sun and moon, respectively

3.6 Ballistic Parameter Determination

The ballistic parameter $B = c_D A/m$ combines all spacecraft information which is relevant for the determination of the along-track drag deceleration, and hence for the corresponding loss of orbital energy and the resulting orbital decay. Mostly, for orbit determination purposes, a lumped expression for B (or its inverse $\beta = 1/B$) is fitted together with an orbit state at epoch. The solve-for parameters are then iteratively improved until a least squares fit of an observed satellite orbit history is obtained. For Salyut-7/Kosmos-1686, following the modelling structure of the FOCUS program, a mean area-to-mass ratio of $\bar{A}/m = 6.27 \times 10^{-3}$ m²/ kg shall be adopted for all sub-

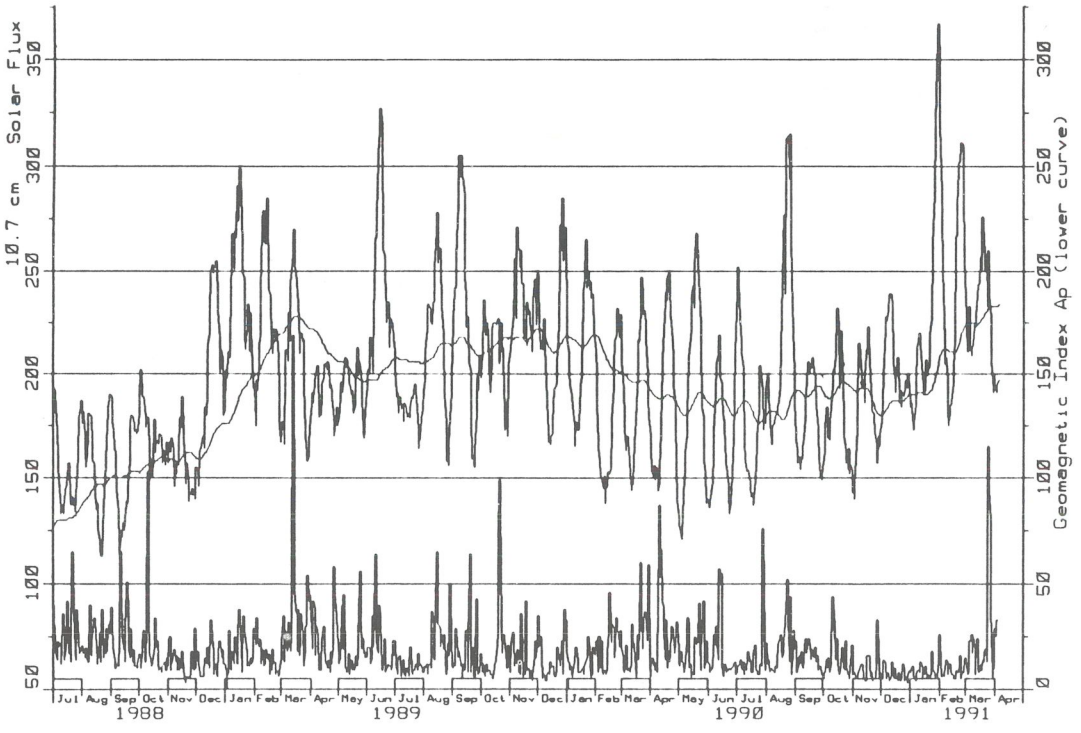

Figure 4. Solar and Geomagnetic Activity Time Record: 10.7-cm solar flux ($F_{10.7}$) daily index and 90-day running mean, and geomagnetic A_p daily planetary index during the decay of Salyut-7/Kosmos-1686.

sequent calculations. The drag parameter c_D is then fitted to best match the observed $\dot{a}(t)$ decay history.

For near-circular orbits (as for Salyut-7/Kosmos-1686), the decay rate of the semimajor axis is approximated to order O(e) by

$$\dot{a} = - c_D \frac{\overline{A}}{m} \rho a V_{atm} \tag{7}$$

Apart from the calibration parameter c_D, the right hand side is given by the adopted area-to-mass ratio $\overline{A}/m$ = const., air density ρ = fct(h, ϕ, λ, UT, τ, t_d, $\overline{F}_{10.7}$, $F_{10.7}$, A_p), semimajor axis a, and the tangential component V_{atm} of the relative S/C velocity through the co-rotating atmosphere.

Within the FOCUS program, the drag perturbation equations for all six Kepler elements are given in analytically tractable expansions up to order e^3 of the eccentricity and order $(\omega_e/n)^3$ of the relative earth rotation frequency (where $\omega_e/n \approx 1/15$). Further perturbation terms due to diurnal density variation ("bulge") and/or due to periodic variations of the aerodynamic cross-section can be optionally merged into these equations, before the averaging operation over 2π of the mean anomaly M is performed, employing the eccentric anomaly E as integration variable (via eq.(2), in order to use integral solutions in terms of modified Bessel functions).

From eq.(7) it is evident that for a constant atmospheric and orbital environment at epoch t one has

$$\frac{\dot{a}}{c_D \overline{A}/m} = \text{const}(t) = C_B(t) \tag{8}$$

and due to $\overline{A}/m$ = const, eq.(8) reduces to

$$\frac{\dot{a}}{c_D} = \text{const}(t) = C_{CD}(t) \tag{9}$$

Three different methods are implemented in the FOCUS program for the tuning of the drag parameter c_D to an observed orbit decay history:

- Single Step Calibration: for given environmental and orbit conditions at time t, and for and arbitrarily defined drag coefficient $c_{1,D}$, a corresponding mean decay rate $\dot{a}_1$ is determined from the averaged drag equations of motion. The ratio $\dot{a}_1/c_{1,D}$ then establishes the 'constant' $C_{CD}(t)$ on the right hand side of eq.(9). If a time history $a(t)$ of the semimajor axis is known from observations, a (parabolic) least squares fit $\tilde{a}(t)$ can be determined (see eq.(3)), and differentiated with respect to time to obtain

$$\dot{\tilde{a}}(t) = c_1 + 2\, c_2 t \tag{10}$$

for the same epoch at which $C_{CD}(t)$ was established. The single step calibration of the spacecraft related drag coefficient $\tilde{c}_D(t)$ is then performed via

$$\tilde{c}_D(t) = \dot{\tilde{a}}(t)\, C_{CD}(t) \tag{11}$$

A draw-back of this technique is its strong sensitivity with respect to temporal perturbations of the environment (solar and geomagnetic activity), and a cross-feed of uncertainties of the fitted $\dot{\tilde{a}}(t)$ via eq.(3) and (10) into the solution (11). Typical 1-σ uncertainties of the fitted decay rate are on the order of 5%, whereas variations in the c_D estimate are about 10% to 15% of its magnitude. If no other a-priori knowledge of c_D is available, then the Sin-

gle Step Calibration method can be employed as an automatic starting procedure, providing initial estimates of c_D to the following, more accurate iteration schemes.

- Iteration by Shooting Method: starting from an observed orbit state $x(t_0) = (a, e, i, \Omega, \omega, M)$ at epoch t_0, the averaged perturbed equations of motion of the six Kepler elements are integrated forward or backward in time to the epoch of another state observation at t_T (with subscript T for target). For the propagation it is assumed that an initial estimate of $c\beta$ is available (either user defined or determined by the Calibration Method), and that a complete history of solar and geomagnetic activities is known over the prediction time span of $\Delta t = t_T - t_0$. For this reference prediction arc, and for a neighbouring arc which is generated with an initial incremental offset of $\Delta c\beta = +0.05\, c\beta$, the resulting semimajor axes $a^0(t_T)$ and $a^1(t_T)$ are used to iterate c_D in order to reach the observed target value of $a(t_T)$. For the i-th iteration, one finds the necessary correction $\Delta c\beta^i$ to the drag coefficient from

$$\Delta c_D^i = -\,(c_D^i - c_D^0)\,\frac{a^i(t_T) - a(t_T)}{a^i(t_T) - a^0(t_T)} \qquad (12)$$

and hence, for the $(i+1)$-th iterate of c_D one gets

$$c_D^{i+1} = c_D^i + \Delta c_D^i \qquad (13)$$

the iteration is terminated after a user defined maximum number of loops i_{max}, or if $\Delta c\beta^i$ is below a threshold accuracy level ε_{CD} of for instance 0.1%. In general, less than 4 iterations are necessary to meet this convergence criterion.

- Iteration by Least Squares Fit: in contrast with the Shooting Method, the Least Squares technique takes full account of all observations of $a(t)$ throughout the propagation interval $t \in [t_0, t_T]$. The initial estimate $c\beta$ is successively improved with the aid of two neighbouring propagation arcs which are generated with symmetrically offset drag coefficients of initially $\Delta c\beta^+ = +\,0.05\, c\beta$ and $\Delta c\beta^- = -\,0.05\, c\beta$. For each of the three arcs, covering all intermediate observation points, the RMS deviations in semimajor axis are computed and used to determine an improved c_D estimate. For the i-th iteration one obtains the following parabolic correction scheme

$$\Delta c_D^i = \frac{\Delta c_D^{i-1}}{2}\,\frac{\Delta a_{RMS}^{i-} - \Delta a_{RMS}^{i+}}{\Delta a_{RMS}^{i+} - 2\,\Delta a_{RMS}^{i} + \Delta a_{RMS}^{i-}} \qquad (14)$$

where Δa_{RMS}^i, Δa_{RMS}^{i+}, and Δa_{RMS}^{i-} are the RMS errors in semimajor axis over the integration interval $\Delta t \in [t_0, t_T]$ for the current estimate of $c\beta^i$ of the drag coefficient, and for the neighbouring values with offset $\pm\,\Delta c\beta^i$, respectively. The update $c\beta^{i+1}$ of the drag coefficient is computed according to eq.(12), applying the same convergence criteria as before. Again, three to four iterations are normally sufficient.

The c_D determination and iteration techniques listed above are given in ascending order of accuracy and also in ascending order of CPU time consumption. In general, the Shooting Method is a good compromise between these conflicting performance parameters (see Tab.2).

In essence, the three c_D determination methods have the following characteristics:

- Single Step Calibration (Tab.2, No.1-3): a robust method, which takes into account the whole $a(t)$ history over a given time span Δt, but does not consider orbit mechanics for the determination of a polynomial least squares fit $\tilde{a}(t)$. Typical RMS errors of the smoothed decay history $\tilde{a}(t)$ are on the order of 5%, while due to temporal perturbations of the atmospheric environment, a typical uncertainty in the calibrated c_D is on the order of 10% to 15%. Due to only two calls to the (drag) perturbation function, the method is very CPU time efficient.

- Iteration by Shooting Method (Tab.2, No.4): uses the full perturbation theory for the forward or backward orbit propagation, but takes into account only the $a(t)$ data at the beginning and at the end of the prediction time span. Hence, the method can be sensitive with respect to bad $a(t)$ data points, whereas atmospheric variations are mostly averaged out, provided that the arc length is selected long enough. For each c_D iteration the method generates one new $a(t)$ history, with one call to the perturbation function at each integration step (with a corresponding increase in CPU time). The c_D results from the Shooting Method showed a very good stability during the re-entry of Salyut-7/Kosmos-1686, and mostly matched the accuracy of results from Iteration by Least Squares Fit ($\Delta c\beta^{MS} \approx 5\%$).

- Iteration by Least Squares Fit (Tab.2, No.5): the draw-backs of the previous techniques are removed largely, since the sensitivity for bad $a(t)$ orbit data, and for bad atmospheric model data ($\bar{F}_{10.7}$, $F_{10.7}$, A_p) is reduced due to RMS fitting and 'low-pass filtering' in the course of the orbit integration. For each c_D iteration the method generates three new $a(t)$ histories, with one call to the perturbation function at each integration step. Hence, this procedure is the least CPU time efficient. The accuracies retained in the c_D estimates are generally on the order of 3% (when compared with a long-term c_D history).

4. Final Re-Entry to Ground

4.1 Prediction of the Final Descent

In the course of the lifetime of a decaying satellite orbit, the perturbation forces due to the non-spherical geopotential, due to airdrag, due to luni-solar third body attraction, and due to solar radiation pressure are dominating the overall perturbation level to a different extent. In a near-earth environment (altitudes 200 to 700 km) the earth oblateness term due to J_2 is generally regarded as the only first order perturbation, while higher zonal harmonics and airdrag are regarded as second order contributions. All other effects are of less than second order (i.e. less than $(J_2)^2$ in magnitude). The formulation of analytically tractable expressions of the

perturbation equations strongly relies on the validity of these assumptions (see 3.1).

In case of a satellite re-entry, the spacecraft sooner or later passes through an altitude regime where the exponentially increasing air density leads to a magnitude of the resulting drag force which is of the same perturbation order as the J_2 earth oblateness effect. At these altitudes (normally around $h \approx 150$km, depending on the ballistic parameter of the spacecraft), the accuracy of analytically derived drag perturbation results strongly deteriorates.

In order to overcome the deficiencies of the semi-analytical orbit prediction technique at low altitudes, the FOCUS program stops its state propagation after trespassing through a user-defined geodetic altitude shell ($h = 170$km in case of Salyut-7/Kosmos-1686), and forwards a derived osculating Kepler state vector at epoch, together with all relevant perturbation parameters and control switch settings to an intermediate result file. This result file is then interrogated by a numerical integration program which continues the propagation of the re-entry trajectory until shortly before impact on ground.

The numerical integrator is a derivative of the USOC software (Unified System for Orbit Computation, Ref.4), with extensions especially for the drag force formulation. The program has the following key features:

- Perturbation Equations: Cowell formulation of the perturbed Newton equations in terms of 6 first order differential equations for each component of the cartesian state vector; reference frame: mean equatorial system of date; perturbation models: GEM-10B geopotential model (used: J_2 to J_7), air densities from MSIS-86 for $h \geq 120$km, US Standard Atmosphere for $h \leq 90$km, and from a bridging function for 120 km $> h >$ 90km, variable drag coefficient c_D = fct(Ma, Kn, Re), co-rotating earth atmosphere, luni-solar third body attraction (point mass model), and solar radiation pressure

- Integrator: Runge-Kutta/Shanks 7/8 single step method for the generation of a starting arc; an Adams-Bashforth/Adams-Moulton (AB/AM) fourth order predictor/corrector multi-step method for the propagation of the cartesian state vector; non-regularised time t used as integration variable, with constant step sizes of $\Delta t = 30$ sec

- Limitations: the propagation of the re-entry trajectory is terminated at a threshold altitude (used: $h = 30$km), where the governing laws of perturbed Kepler motion become invalid; this criterion is marked by a decrease of the orbital energy to a level, where the aerodynamic forces are in balance with the zero-th order central gravitational attraction term

The unconventional use of a multi-step method for the strongly perturbed re-entry path, rather than the use of a single-step (Runge-Kutta) method with step size control, can be justified by verification runs which demonstrate that a 4-th order Adams-Bashforth integrator with small enough step size (30 sec) meets the accuracy of a multi-step method, and shows a high numerical stability.

Since from $h \leq 30$km altitude the spacecraft is in an almost vertical fall, there is only a minor dispersion of the impact point during the remaining seconds of the flight. Hence, no attempt has been made to perform another transition from the strongly perturbed Kepler orbit phase to an aerodynamic flight phase for the integration to ground level. The following results of COIW times and locations shall thus refer to the passing through a geodetic altitude of about 30 km.

4.2 Air Density Model

For the numerical integration of the re-entry trajectory downward from 170 km, air densities are determined from the MSIS-86 model and from the US Standard Atmosphere 1976 (USSA-76), for the thermospheric phase and the homospheric phase, respectively. The atmospheric transition zone between the altitude regimes of these two models is covered by a smooth bridging function. The air densities with decreasing altitude are determined as follows:

- Thermosphere ($h \geq 120$km): MSIS-86 (identical to CIRA-86 in this region), a dynamic atmosphere model based on analytical models of the temperature profile according to Bates, and of concentration profiles of the major atmospheric constituents (O, O_2, N, N_2, He, H, Ar) according to Walker; the model includes variations with geodetic altitude h, geodetic latitude ϕ, geographic longitude λ, universal time UT, local solar time τ, day of the year t_d, actual and mean solar activity $F_{10.7}$ and $\bar{F}_{10.7}$, and geomagetic activity A_p; total density ρ is computed from a mean of the individual concentration profiles, weighted by the respective molar masses.

$$\rho_{MSIS} = \text{fct}(h, \phi, \lambda, UT, \tau, t_d, \bar{F}_{10.7}, F_{10.7}, A_p) \quad (15)$$

- Homosphere ($h \leq 90$km): US Standard Atmosphere 1976 (USSA-76), a static, solely height dependent model which provides total densities as a function of geodetic altitude for mid latitudes.

$$\rho_{USSA} = \text{fct}(h) \quad (16)$$

- Transition Regime (120 km $\geq h \geq$ 90km): total densities are computed from a weighted mean of ρ_{MSIS} and ρ_{USSA}

$$\tilde{\rho} = w_{MSIS}\,\rho_{MSIS} + (1 - w_{MSIS})\,\rho_{USSA} \quad (17)$$

where the weighting factor $w_{MSIS}(h) \in [0, 1]$ is defined by the following expression for the altitude shell $h_{120} \geq h \geq h_{90}$

$$w_{MSIS}(h) = \frac{1}{2}\cos\left(\pi \frac{h_{120} - h}{h_{120} - h_{90}}\right) + \frac{1}{2} \quad (18)$$

At $h = 120$ km, $\tilde{\rho}$ starts off as a weak function of the non-altitude parameters, and as altitude decreases towards 90 km the density profile becomes totally static. During tests, the MSIS and USSA density models were found to be in good agreement within the zone of altitude overlap, and maximum discrepancies were generally less than 10%. The use of eq.(17) assures a smooth altitude profile of the air density $\rho(h)$, and also of its derivative $d\rho(h)/dh$.

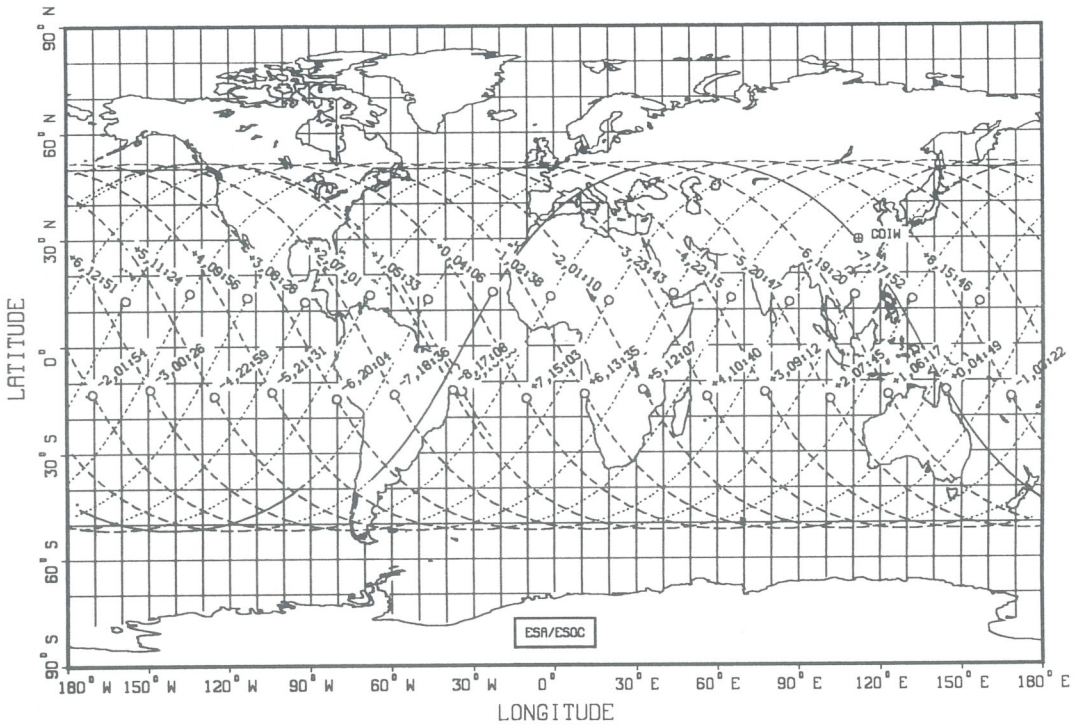

Figure 5. Predicted Groundtracks on Re-Entry Day of Salyut-7/Kosmos-1686: Ascending and descending node passes for ± 7 groundtracks, centred on the predicted re-entry COIW at 04:33 UTC on Feb.07 (forecast from Feb.06 11:00 UTC).

4.3 Drag Coefficient Model

The drag coefficient of a spacecraft is a scaling parameter in the equation of the aerodynamic drag deceleration $\vec{a}_{atm}$ which accounts for the interaction of the satellite with the atmosphere environment.

$$\vec{a}_{atm} = - c_D \frac{\overline{A}}{m} \rho V_{atm} \vec{V}_{atm} \tag{19}$$

where $\overline{A}/m$ is a conventional mean area-to-mass ratio, and $\vec{V}_{atm}$ is the relative velocity through a moving atmosphere (co-rotation and wind patterns).

In the most general case, c_D is a function of spacecraft parameters (geometry, attitude, surface material properties, surface temperature), of atmospheric conditions (composition, temperature, mean free path length, etc.), and of orbit path constraints (velocity and position).

Provided that the spacecraft attitude does not change significantly, and provided that the aerodynamic flow regime is of the free-molecular type, the magnitude of the drag coefficient can be regarded as almost constant. For the Salyut-7/Kosmos-1686 configuration, these conditions were well approximately for most of the orbital lifetime, when the object was in a gravity-gradient stabilisation mode (see 3.3), and when the orbit altitude was high enough to maintain $Kn_\infty = \lambda_\infty / d_{S/C} > 1$ (where Kn_∞ is the Knutsen number, λ_∞ is the free molecular pathlength, and $d_{S/C}$ is a characteristical length of the spacecraft). Hence

$$c_D \approx const = c_0^{Kn} \tag{20}$$

if $Kn_\infty > 1$. Thereafter, as the orbit altitude decreases, a transition zone to hypersonic continuum flow is entered, where the drag coefficient can be modelled via a logarithmic profile (where $Kn_\infty = fct(h)$).

$$c_D = c_1^{Kn} + c_2^{Kn} \log_e(c_3^{Kn} Kn_\infty) \tag{21}$$

if $0.02 \leq Kn_\infty \leq 1$. During the phase of hypersonic continuum flow, another constant c_D level is obtained (about 50% lower than in free-molecular flow).

$$c_D \approx const = c_0^{Ma} \tag{22}$$

if $0.02 \geq Kn_\infty$ and $Ma_\infty \geq 5$. The following phase of supersonic and transsonic continuum flow can be approximated by a function of the altitude dependent Mach number $Ma_\infty = fct(h)$.

$$c_D = c_1^{Ma} + c_2^{Ma} (Ma_\infty - 0.4)^{**} c_3^{Ma} \times \exp[-c_4^{Ma}(Ma_\infty - 0.4)] \tag{23}$$

if $0.02 \geq Kn_\infty$ and $0.8 \leq Ma_\infty \leq 5$. If the re-entry trajectory integration is performed to ground impact, then in its last (subsonic) phase, the drag coefficient becomes dependent on viscous interactions, and hence on the Reynolds number $Re_\infty = fct(h)$.

$$c_D = c_1^{Re} (Re_\infty)^{**} c_2^{Re} \tag{24}$$

if $0.02 \geq Kn_\infty$ and $0.8 \geq Ma_\infty$. These dependencies c_D = fct(Kn, Ma, Re), with the underlying altitude functions Kn(h), Ma(h), and Re(h) from the US Standard Atmosphere, are incorporated in the numerical re-entry prediction software. The model constants in the above equations are only available for spherical shapes and for cylinders, with their longitudinal axis perpendicular to the airflow. For Salyut-7/Kosmos-1686 the latter

model was used as reference. In order to allow for a smooth transition from the calibrated c_D result of the semi-analytical propagator to the c_D model of the numerical re-entry prediction program, a bridging function similar to eq.(18) is employed.

Since the Mach number ($Ma = V_{atm}/V_{sound}$) and the Reynolds number ($Re = V_{atm}d/\nu$) are a function of geodetic latitude (via $V_{sound}(h)$ and kinematic viscosity $\nu(h)$) and of aerodynamic velocity V_{atm}, the free fall of a space object in the lower atmosphere (after its loss of orbital energy) can be determined by iteratively solving the following equation for the equilibrium descent velocity V_{atm}.

$$(V_{atm})^2 \approx (\dot{h})^2 = 2 \frac{m}{\bar{A}} \frac{g(h)}{\rho(h)\, c_D(h, V_{atm})} \qquad (25)$$

where $g(h)$ is the central gravitational acceleration of the earth, and $\rho(h)$ is the local air density.

For Salyut-7/Kosmos-1686, with a mean surface load of $m/\bar{A} = 159.5$ kg/m², the equilibrium free-fall velocity at altitudes $h = 30$ km, 20 km, and 10 km is on the order of $\dot{h} = 330$ m/s, 100 m/s and 70 m/s, respectively. These estimates from eq.(25) are also confirmed by numerical re-entry prediction results at the limiting altitude of 30 km.

5. Re-Entry Prediction Results

5.1 State Input Accuracy

A generally good agreement between TLEs as determined by USSpaceCom directly, and as derived from tracking data sources outside the US Space Surveillance Network could be observed for most of the Salyut-7/Kosmos-1686 re-entry campaign. For a subset of these data, from 1991-Jan-26 02:34 UTC to Feb-01 12:00 UTC, a more detailed analysis shall be performed. This data arc was used to retro-fit the drag coefficient for prediction run no.23 (out of a total of 37 predictions).

The TLE notation shall within this discussion be applied to all orbit state data sources, and error characteristics shall be provided for the entire 6.5 day batch after transformation to a common format (singly averaged Kepler elements in a mean system of date). It should be noted that the exclusive analysis of genuine USSpaceCom data would generate a more uniform error log, but the large share of data from Germany (FGAN) and from the USSR suggests to proceed this way.

To get a feeling for the accuracy of the TLE input data, a low order (order 3) time polynomial is fitted through the "observations" of the mean Kepler states within the time batch. This least squares fit, which mimics a low-pass filter, does not consider orbit dynamic constraints. The results of the corresponding RMS and maximum mismatches over the 6.5 days test arc are summarised in Tab.1 . These figures should be seen in the light of the simplified low order smoother, and of the inhomogenious data sources. The upper half of the table shows error statistics for all available data (from any source) within the given time span. These results shall be discussed first.

For the semimajor axis a, the residuals of $\Delta a_{max} = 261\ m$ and $\Delta a_{RMS} = 140\ m$ of the third order polynomial fit compare favourably with $\Delta a_{max} = 497\ m$ and $\Delta a_{RMS} = 153\ m$ from Tab.2 . In the latter case, starting from epoch Feb-02 12:00 UTC, a backward RMS fit of the mean semimajor axis by c_D iteration was performed, keeping the initial mean state (and thus $a(t_0)$) fixed. For this retro-fit a full orbit perturbation model was employed. The magnitude of the RMS residuals of the $a_{TLE}(t)$ data is about 3 to 4 times of what can be achieved from an orbit determination over a short arc of radar observations of about 6 hours (4 consecutive passes). Due to its direct impact on orbital period and acquisition times, the semimajor axis is known with very good relative accuracy, and from the analysed data batch, no systematic errors (biases) are noticeable for any of the data sources.

TLE Data Dispersion vs. Low Order Smoother

Mean Kepler Elements	Combined Data Sources	
	Max	RMS
semimajor axis (m)	261	140
eccentricity (-)	2.58e-4	7.51e-5
inclination (deg)	6.96e-3	3.45e-3
R.A. of asc. node (deg)	3.65e-2	1.12e-2
arg. of perigee (deg)	53.10	13.54

Mean Kepler Elements	Optimised Data Sources	
	Max	RMS
semimajor axis (m)	222	131
eccentricity (-)	9.01e-5	4.81e-5
inclination (deg)	3.81e-3	1.99e-3
R.A. of asc. node (deg)	1.17e-2	5.48e-3
arg. of perigee (deg)	10.38	4.30

Table 1. Error statistics of TLE derived mean Kepler states: The max. and RMS errors were derived from a low order (order 3) polynomial smoother, applied to a data arc between 26-Jan-91 and 02-Feb-91 (35 data records). The upper half of the table refers to a batch including all available data (6 sources), the lower half considers only a subset of data sources (3 sources).

As a consequence of the near circular orbit of Salyut-7/Kosmos-1686, the eccentricity vector, and hence the eccentricity $e(t)$ and argument of perigee $\omega(t)$ are highly unstable. This results in an RMS error of $\Delta e_{RMS} = 7.51 \times 10^{-5}$ (10% to 15% of its magnitude), and $\Delta\omega_{RMS} = 13.54°$. The maximum errors are larger by a factor of 3 to 4.

The components of the inclination vector, and hence the orbital inclination $i(t)$ and the right ascension of the ascending node $\Omega(t)$ show a very stable time characteristic. Their RMS errors are on the order of $\Delta i_{RMS} = 3.45° \times 10^{-3}$ and $\Delta\Omega_{RMS} = 1.12° \times 10^{-2}$, with the corresponding maximum excursions larger by a factor 2 and 3, respectively.

In general, the most consistent sets of TLEs came from USSpaceCom and from FGAN, when using their orbit

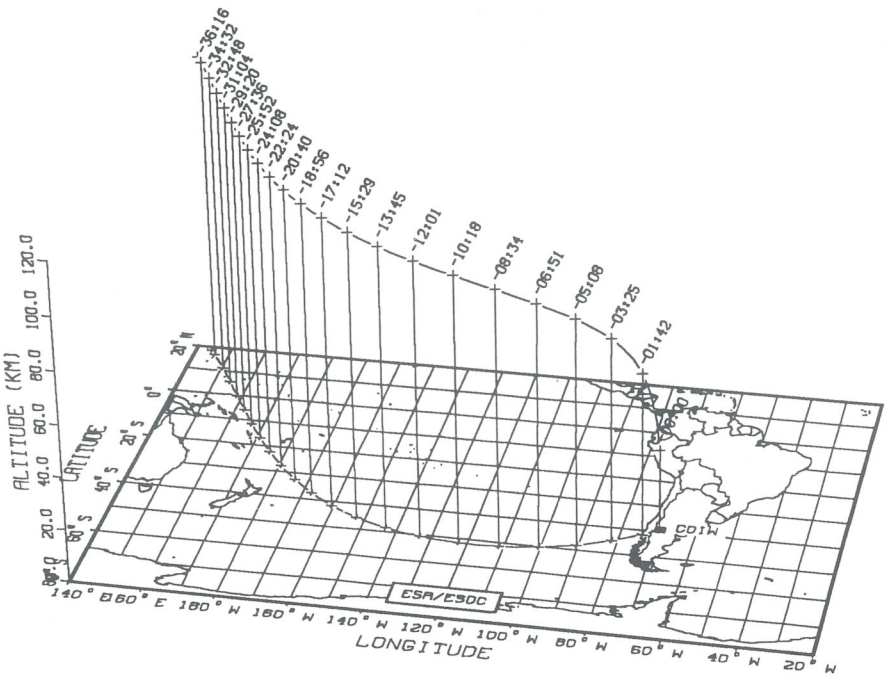

Figure 6. Salyut-7/Kosmos-1686 Final Descent Altitude Profile: The COIW re-entry time (Feb.07 03:45 UTC) and location (69.7°W and 39.3°S) were determined after availability of the TLE data from node crossing at 02:31 UTC (see Tab.4).

determination results from the central pass(es) of 4 to 5 consecutive overflights. Also the ESOC orbit determination results from FGAN range, range-rate, and angular measurements (corrected by FGAN for atmospheric effects) fit well into the USSpaceCom orbit state histories. When using these reduced sources of data, the TLE data consistency is much improved (see bottom half of Tab.1). Except for the semimajor axis with an RMS reduction of only 6%, all other RMS errors are cut by 35% to 68% of their magnitudes from the combined data source solution.

Orbital elements which were received via IKI also had a high intrinsic accuracy. The translation of the provided nodal periods into equivalent semimajor axes based on eq.(1), however, introduced a bias which increased as altitude decreased. This was due to a misinterpretation of T_N as the 'osculating' nodal period, whereas a-posteriori T_N was identified as the time difference between the current and the preceding node pass. Hence, the IKI data sets contained information on the osculating semimajor axis a only in terms of an integral quantity, referring to an epoch other than the current node crossing. The decryption of this datatype would require knowledge on the density and ballistic parameter model which was used for the orbit determination. Such information was not available in time for the Salyut-7 final re-entry prediction. Currently, however, procedures are developped to recover full Kepler state information from the IKI/MCC data type.

5.2 Ballistic Parameter Uncertainties

Three different procedures for the determination of the ballistic parameter of a spacecraft were already outlined in chapter 3.6 : single step calibration, iteration by shooting method, and iteration by RMS error minimisation. In all of these procedures, the time history of the semimajor axis $a(t)$ is used as an indicative of the deduction of orbital energy due to airdrag, which is a linear function of the instantaneous ballistic parameter $B(t) = c_D \bar{A}/m$.

In an attempt to extract periodic variations of the drag coefficient c_D from observed time histories $a(t)$, a batch of data between 10-Dec-1990 and 15-Jan-1991 was fitted by a low order polynomial (order 2, covering rate and rate-rate of change of the semimajor axis). From an inspection of the time evolution of the residuals, a periodic signature became apparent. Fitting of the residuals for the 36 day arc resulted in a period of 29.65 days and an amplitude of 0.224 km/day for a deduced correction term $\Delta\dot{a}(t)$ of the decay rate $\dot{a}(t)$. This corresponds to 14% of the decay rate of 1.633 km/day on 15-Jan-1991. Though the 29.65 day period is close to the 27 day rotation period of the sun (with a "light-tower effect" from the co-rotating sun spots), the correlation of $\Delta a(t)$ and solar activity $F_{10.7}(t)$ is not straight forward. The observed periodicity has also some correlation with the rotation of the line of nodes which has a period of 65.2 days. Performing a similar fit for a subsequent data arc resulted in a reduction of the c_D variation period by about 10%, with a much increased amplitude. Due to the limited predictability of a periodic $c_D(t)$ correction function, the incorporation of this approach in the re-entry prediction procedure was declined.

In Tab.2 an alternative approach to a long arc $a(t)$ data fit is shown. Using a 4th order polynomial fit (order 1 to 2 accounting for rate and rate-rate of change of the semimajor axis, and order 3 to 4 covering harmonic variations of the ballistic parameter), a 29 day arc can be matched with an RMS residual of $\Delta a_{RMS} = 208$ m. A corresponding 2nd order fit showed an RMS error of 1425 m.

Determination of c_d by Different Techniques						
Run No.	Data Arc Extent		Type of $a(t)$ Fit	$a(t)$ Residuals		Type of c_D Fit	Fitted c_D
	From	To		Max (m)	RMS (m)		
1	Jan.01 00:02	Feb.01 12:00	4th degree time polynomial (67 data points used)	476	208	single step calibration (via eq.(11) for Feb.02 12:00)	1.73
2	Jan.26 02:34	Feb.01 12:00	2nd degree time polynomial (35 data points used)	406	232	single step calibration (via eq.(11) for Feb.02 12:00)	1.76
3	Jan.26 02:34	Feb.01 12:00	3rd degree time polynomial (35 data points used)	261	140	single step calibration (via eq.(11) for Feb.02 12:00)	1.97
4	Jan.26 02:34	Feb.01 12:00	backward shooting method (2/35 data points used)	515	157	iterative calibration (via eq.(12) for point 1 and 35)	1.93
5	Jan.26 02:34	Feb.01 12:00	RMS minimisation method (35 data points used)	497	153	iterative calibration (via eq.(14) for all data points)	1.92

Table 2. Comparison of c_D estimation techniques: For Salyut-7/Kosmos-1686 lifetime predictions the drag coefficient was exclusively determined by the shooting or RMS minimisation techniques (which provide best accuracy).

With the approach of the final re-entry, drag perturbations and their effect on altitude and semimajor axis increase strongly. The times spans of $a(t)$ observations which are used to calibrate the drag coefficient must be reduced accordingly, in order to be able to follow short term trends. Likewise, due to increasing changes of the altitude rate and rate-rate, the order of the reference polynomial fit should be increased from 2 to 3. For a 6.5 day data arc (from $t_{entry} - 11d$ to $t_{entry} - 4.5d$) a comparison between Tab.2 no.2 and 3 shows a corresponding reduction of Δa_{RMS} from 232 m to 140 m.

The use of the Single Step Calibration of the drag coefficient $c_D(t)$ by matching of observed decay rates $\dot{a}(t)$ is very sensitive with respect to temporal changes of the drag environment (e.g. solar and geomagnetic activity, see 3.6). During the Salyut-7/Kosmos-1686 re-entry prediction campaign this procedure has only be used for the generation of initial estimates of c_D as starting conditions for the more precise calibration by shooting and RMS minimisation.

Tab.5 shows an example of the c_D calibration by the shooting technique. Hence, the perturbed orbit is integrated, starting with a mean orbit state on 01-Feb-1991, 12:00 UTC, and propagating backwards to a target epoch on 26-Jan-1991, 02:34 UTC. The propagation is repeated, and the drag coefficient is adjusted (via eq.(12,13)) until $a(t)$ at the target epoch is matched with sufficient accuracy, or until changes of c_D fall below a given threshold. The RMS error Δa_{RMS} of the residuals for the present case is 157 m, with a corresponding $c_D = 1.93$. Applying the RMS minimisation technique on the same data arc results in $\Delta a_{RMS} = 153$ m, and $c_D = 1.92$ (see eq.(14) and Tab.2). The slightly increased RMS error of the Shooting Method and RMS Minimisation Method as compared with the third order polynomial fit is due to the initial conditions (and hence $a(t_0)$) being fixed for the first runs, and being adjusted for the latter one.

For the lifetime and decay prediction of Salyut-7/Kosmos-1686 the determination of the drag coefficient from observed decay histories was mostly performed by means of the Shooting Method which proved to be very robust and insensitive with respect to sparse data and isolated data of poor quality. Moreover, this technique allows to select start and end conditions from the same data source, calibrates c_D for this source, and monitors mismatches of intermediate data points (from arbitrary sources) with respect to the fitted $a(t)$ history. The length of the fitted data arcs must be reduced from about 30 days at high altitudes to 1 or 2 days shortly before re-entry.

The calibrated drag coefficient during the last two months of the orbital lifetime of Salyut-7/Kosmos-1686 was consistently between $c_D = 1.85$ and 2.15 (with the exception of the last orbits). The corresponding ballistic parameter range is $B = c_D \bar{A}/m = 5.82 \times 10^{-3}$ to 6.77×10^{-3} m²/kg. These results conform well with independent computations of the free-molecular aerodynamics of the Salyut complex by means of Pike's method (on-going ESA contract with HTG/Goettingen).

5.3 Lifetime Prediction Uncertainties

For the analysis of error contributions to lifetime predictions the following sources of uncertainty can be distinguished (in ascending order of significance):

- Simplified assumptions in the implemented orbit and environment models
- Uncertainties in the orbit state determinations (bad initial conditions)
- Poor predictability of short term solar and geomagnetic activity variations
- Limited knowledge on the geometry, mass, and attitude of the spacecraft

The FOCUS orbit generator (see 3.1), which is employed for the long term lifetime predictions, is propagating singly averaged 1-st order (J_2) mean Kepler elements. As such, the short periodic altitude variations at half the nodal period and amplitudes of about Δh (km) $\approx 2 \sin^2 i$ are not considered for the computation of the air density profile along the orbit. Further simplifications are used in the formulation of the diurnal density bulge, and of the drag equations of motion, where expansions in eccentricity are truncated after e^3. All other perturbation effects (geopotential, luni-solar, and radiation pressure) are solved for in finite expansions with no truncation errors. For the numerical final re-entry prediction with the USOC program (used after trespassing 170 km altitude level) implementation errors of the perturbed equations of motion can be neglected.

Both, the semi-analytical and the numerical technique use the MSIS-86 model of the thermosphere down to 90 km, and the US Standard Atmosphere 1976 (USSA-76) from 0 to 120 km altitude. A bridging function is providing a smooth transition in the overlapping altitude band (see 4.2). The RMS error of the model(s), according to their authors, should be on the order of 10% to 15% for known activity conditions.

The accuracy of orbit state input data (with due regard to the semimajor axis) has been investigated in 5.1 . An uncertainty of $\Delta a_{RMS} = 100$ m to 200 m can be expected above about 200 - 250 km altitude. During the final descent, larger dispersions can be noticed.

For long term lifetime forecasts a good model for the expected solar and geomagnetic activity over the prediction time span is essential. In 2.1 the ESOC modelling approach is briefly explained, and in Fig.4 the actual observation record of $\bar{F}_{10.7}$, $F_{10.7}$, and A_p for the last 3 years of Salyut's orbital lifetime is charted. In can be noticed that between Sep-1990 and mid Jan-1991 the solar activity was high, but at a steady level, with harmonic variations of amplitudes of about $\pm$ 60 at periods close to the solar rotation cycle of 27 days. By the end of Jan-1991, the $F_{10.7}$ level built up to a maximum of 267 (on 30-Jan-1991) within one week. At this time, however, the Salyut complex was already at an altitude of 222 km, and descending at more than 4 km/day. Due to the specifics of the vertical structure of the thermosphere, solar activity variations have there largest impact at altitudes around 500 to 600 km. Their influence on temperature and total density is diminishing as altitude decreases towards 120 km, where the transition to the near-static homosphere starts. Consequently, the lifetime expectance of Salyut-7/Kosmos-1686 was not strongly affected by the record solar activity peak of the current solar cycle (equalising the peak of the previous cycle 21 in 1979). Fig.4 also reveals that during the lifetime prediction activities no geomagnetic storms occurred. Most A_p observations are well below 100 (out of a possible range of values up to 400). For the lifetime and re-entry prediction of the Salyut-7 complex, solar and geomagnetic forecast uncertainties were considered by adding $+1\sigma$ to the predicted means of $\bar{F}_{10.7}(t)$ and $A_p(t)$ (i.e.: there is a 84% chance that this level will not be exceeded).

A dominating source of uncertainty for lifetime predictions of complex spacecraft (especially in the final phase of re-entry) is the estimated ballistic parameter B (see 5.2). A retro-fit of B with respect to "observed" orbit states of Salyut-7/Kosmos-1686 resulted in stable estimates of the calibrated drag coefficient c_D of about $2.0 \pm 0.15 (\pm 7.5\%)$ until one day before re-entry.

During the last orbits c_D was estimated at 2.42 . For long term lifetime predictions the last calibrated drag coefficient was used, with a 10% uncertainly added to determine the re-entry time window. Due to the large uncertainty in attitude and configuration of the object in its final descent (a solar array of Salyut-7 was bent against the cylindrical body, and the whole configuration was tumbling and spinning), a 20% margin on c_D was allowed for to simulate an along track debris trace.

5.4 Re-Entry Time Window Uncertainties

Fig.3 summarises the Salyut-7/Kosmos-1686 lifetime prediction results from 17-Nov-1990 up to 06-Feb-1991. In a diagram of predicted re-entry date versus epoch of last available TLE data ($\approx$ date of prediction) the solid line marks the nominal COIW (Centre Of Impact Window) times, and the dashed lines indicate the width of the re-entry time window. Vertical bars more clearly mark the dates at which predictions were performed and their time separation. Early updates are with a spacing of about one week, while during the last 10 days of the orbital lifetime predictions were performed once per day, and on the last day each new orbit state was processed to generate an improved COIW time and location.

The purpose of a re-entry time window indication is to ascertain that any nominal COIW prediction at a given date remains within the uncertainty time windows of all previous predictions. The time window shall thus indicate maximum possible shifts in re-entry date under extreme conditions. Fig.3 demonstrates that this requirement was met during the whole Salyut-7 re-entry campaign, and that the assumptions for generating the impact time window ($B + 10\%$ and $\bar{F}_{10.7}(t) + 1\sigma$ (84% confidence level)) were justified. The assumed maximum values of B and $\bar{F}_{10.7}$ were used to compute the lower end of the time window. The upper portion of the envelope was taken as symmetric with respect to the nominal COIW time forecast. This is a strong simplification since symmetric offsets in B and $\bar{F}_{10.7}$ do not produce a symmetric re-entry time window. The overshoot branch of the envelope can be elongated by 30% or more with respect to the undershoot branch (due to extended orbit resident times, and the exponentially diverging drag environment as compared with a maximum drag orbit). The time window results which ESOC released through their "Prediction Bulletins" were mostly corrected for overshoot uncertainties by adding some 30% to the computed time window based on the previous assumptions (see insert in Fig.3 which summarises the forecasts from the "Prediction Bulletins").

5.5 Monitoring the Final Re-Entry

The long term lifetime prediction of Salyut-7/Kosmos-1686 was performed with a combined semi-analytical prediction to a 170 km limiting altitude, and a subsequent numerical integration until shortly before impact (30 km terminal altitude). The results of this approach are illustrated in Fig.3 . In the final re-entry phase, during the last day of the lifetime, when the complex was well below 170 km altitude, the orbit propagation was done purely numerically. The semi-

Re-Entry Prediction Information vs. Time

Prediction Source	Re-Entry Predictions (times in UTC)	
	Received at ESOC	Re-Entry Pred. (COIW)
NASA GSFC	01-Feb 14:58	06-Feb 21:33
ESOC MAS	02-Feb 04:27	06-Feb 22:30
CNES CST	03-Feb 11:33	06-Feb 04:00
ESOC MAS	04-Feb 10:30	07-Feb 01:37
NASA GSFC	04-Feb 16:04	07-Feb 03:38
CNUCE CNR	04-Feb 19:43	07-Feb 03:17
CNES CST	05-Feb 04:27	06-Feb 18:23
ESOC MAS	05-Feb 10:00	07-Feb 02:23
NASA GSFC	05-Feb 15:05	07-Feb 03:05
ESOC MAS	06-Feb 11:33	07-Feb 03:50
RAE	06-Feb 11:38	07-Feb 04:30
CNUCE CNR	06-Feb 12:50	06-Feb 22:26
NASA GSFC	06-Feb 14:09	07-Feb 03:28
CNUCE CNR	06-Feb 16:51	07-Feb 01:24
NASA GSFC	06-Feb 16:58	07-Feb 04:14
CNES CST	06-Feb 17:00	07-Feb 05:00
ESOC MAS	06-Feb 19:47	06-Feb 04:19
CNUCE CNR	06-Feb 22:05	07-Feb 04:43
CNES CST	06-Feb 22:15	07-Feb 04:38
IKI IAM	06-Feb 23:37	07-Feb 04:40
NASA GSFC	06-Feb 23:44	07-Feb 04:05
ESOC MAS	07-Feb 01:00	07-Feb 04:50
IKI IAM	07-Feb 01:02	07-Feb 04:38
IKI MCC	07-Feb 01:02	07-Feb 04:20
CNUCE CNR	07-Feb 01:07	07-Feb 04:00
IKI MoD	07-Feb 01:57	07-Feb 04:00
IKI MCC	07-Feb 02:22	07-Feb 03:57
IKI IAM	07-Feb 04:00	07-Feb 03:37
ESOC MAS	07-Feb 04:20	07-Feb 04:29
IKI MoD *	07-Feb 04:34	07-Feb 03:47
ESOC MAS *	07-Feb 13:00	07-Feb 03:45

Table 3. Forecasts of the Final Decay of Salyut-7/Kosmos-1686: Timeline of re-entry prediction results as received at ESOC. All times are in UTC of year 1991, with markers (*) indicating a post-decay reconstruction of the re-entry time and location with data which only became available after the event.

analytical technique was used only to check on the currently used drag coefficient c_D (and thus on the ballistic parameter B) by retro-fitting the orbit with respect to previous data. The Salyut-7 station passed the 170 km altitude level in the early morning of 06-Feb-1991.

Available Orbit Determinations vs. Time

Information Source	Orbit Element Information (times in UTC)	
	Ascending Node Pass	Time of Reception
USSpaceCom	06-Feb 11:57	06-Feb 16:18
USSpaceCom	06-Feb 14:52	06-Feb 16:18
USSpaceCom	06-Feb 16:20	06-Feb 21:32
IKI MoD	06-Feb 19:15	06-Feb 20:51
USSpaceCom	06-Feb 19:15	06-Feb 22:57
IKI MoD	06-Feb 20:42	06-Feb 22:41
IKI MoD	06-Feb 22:09	07-Feb 00:28
IKI MoD	07-Feb 01:04	07-Feb 02:22
USSpaceCom*	07-Feb 01:04	07-Feb 03:37
IKI MoD *	07-Feb 02:31	07-Feb 03:51
USSpaceCom*	07-Feb 02:31	07-Feb 06:29

Table 4. Salyut-7/Kosmos-1686 Orbit Determinations.: Timeline of orbit determination results as received at ESOC. All times are in UTC of year 1991, with markers (*) indicating that data were received after the re-entry.

For the last week of the orbital lifetime Tab.3 provides a time record of predicted COIW times, sorted in ascending order of times at which the forecasts reached ESOC, and indicating the establishment from which the result was received. Looking at a moving mean of the COIW results (with special weight on USSpaceCom/GSFC and USSR-MCC/IKI), one can notice that the general trend goes from a COIW in the late evening of Feb.06 (by Feb.01) towards Feb.07 between 04:15 and 04:30 UTC (by Feb.06), at a "mean rate" of about 1 h/day. This forward trend only reversed shortly before midnight of Feb.06, when forecasts started to settle around Feb.07 04:00 with steadily decreasing time windows down to $\pm$ 15 min. Only by the time when the first fragments reached the ground, ESOC received a prediction from IKI for a COIW epoch at 03:37 UTC. This final forecast was corrected to 03:47 UTC immediately after re-entry (received at ESOC at 04:34). Later, TASS published a COIW time at 03:45 UTC for a location at 34.9°S and 63.8°W. These results were later supported by visual observations of falling debris over Argentina.

The long-term ESOC forecasts for the Salyut-7/Kosmos-1686 re-entry, and the associated uncertainties according to Fig.3 agree well with earlier results from USSpaceCom and IKI/MCC. This good agreement is also noticeable for the prediction record of the last week before decay, from Feb.01 up to about 19:00 UTC on Feb.06 (see Tab.3). A cross-check with Tab.4 shows which TLE orbit information from which source was available by the time of the ESOC forecasts. As the re-entry came closer, the response times between orbit determination and the transmission of TLE results to ESOC became much shorter for the IKI/MCC data than for the USSpaceCom/GSFC data. The USSR elements were mostly available within one revolution after the orbit determination, whereas the delivery time of US data was 2 to 3 times longer. This time shift re-

sulted in an artificial weighting of the IKI/MCC orbit information within the ESOC re-entry prediction process.

Up to Feb.05 (node crossing at 09:37 UTC) the semimajor axis and hence the altitude information from the IKI/MCC state vectors matched well with USSpaceCom and FGAN tracking data, with offsets of about +200 m with respect to a retro-fitted arc. The calibrated c_D at this time was 1.935, and at the same level as for previous fits. The next state vectors from IKI/MCC were obtained for ascending nodes on Feb.06 at epoch 06:07 and 09:02 UTC, a later comparison with FGAN, ESOC and USSpaceCom orbit determination results from epochs between 11:00 and 16:20 UTC revealed a divergent tendency, and maximum offsets with respect to a matched orbit of 560 m and about 1000 m, respectively. Due to the timely availability and sufficient number of FGAN and USSpaceCom state vectors, the ESOC re-entry prediction forecasts up to this point (up to Feb.06, 19:47 UTC issue of the "Prediction Bulletin No.11", see insert in Fig.3) were in good agreement with COIW times indicated by USSpaceCom and IKI/MCC. Thereafter, there was only one additional state vector from USSpaceCom (for node crossing 19:15 UTC) which reached ESOC before the actual decay (available at 23:00 UTC). Subsequent ESOC predictions were more and more dominated by the information of a total of 4 state vectors from IKI/MCC which were provided for 4 consecutive node crossings between Feb.06 19:15 and Feb.07 01:24 UTC. Processing of this information resulted in a forward shift of the COIW time up to 04:50 UTC. At the time of release of this result (01:00 UTC), this was an overshoot by 45 min, 30 min, and 12 min with respect to the forecasts from USSpaceCom/GSFC, IKI/MCC, and IKI/IAM (see Tab.3).

The next USSpaceCom TLE set to arrive was from epoch 01:04 UTC, and reached ESOC at 03:37 UTC. It supplemented the information of a state vector from epoch 19:15 UTC from the same source, and indicated that there was a systematic bias between the IKI/MCC and the USSpaceCom orbit altitude information of about +1500 m (see 5.1 for an explanation). At this point it became evident that the two data sources could not be processed in a common batch, and that c_D drag coefficients had to be determined for each source separately. A USSpaceCom-only solution for c_D by iteration between TLE state vectors of epoch Feb.07 01:04 and Feb.06 19:15 UTC provided a drag coefficient of 1.902, and a COIW time at 04:29 UTC (moving backward with respect to the previous forecast).

The German FGAN tracking station would have acquired the Salyut-7 compound at 04:09 UTC. Salyut-7, however, was at that time reported to have decayed over Argentina, on a northbound track around 03:47 UTC. At this time, ESOC received another state observation from IKI/MCC for the preceeding ascending node pass at 02:31 UTC. Using this information, and retro-fitting the orbit to an IKI/MCC state vector on Feb.06 19:15 UTC, resulted in a calibrated c_D of 2.364 and a COIW "forecast" of 03:36 UTC. Note that this result is closely matching the last IKI/IAM forecast of 03:37 UTC given in Tab.3.

The final USSpaceCom TLE set for the last node pass at 02:31 UTC arrived at ESOC at 06:29 UTC, and was employed for a retro-fit of c_D to a target state on Feb.06 19:15 UTC from the same data source. The computed $c_D = 2.420$ corresponded to a 27% increase with respect to the previous USSpaceCom-only solution, and resulted in a COIW time at 03:45 UTC. This re-entry time, and the corresponding COIW location at 39.3°S and 69.7°W fit well with the IKI/MoD and USSpaceCom/NASA post mortem COIW reconstructions.

6. Summary and Conclusions

The orbital decay of Salyut-7/Kosmos-1686 proved to be an example for good international co-operation in the event of a global threat from a large size re-entry object. Most of the recommendations of a previous Re-Entry Workshop, organised by ESA in 1985 (Ref.9), were followed even beyond original expectations. This was particularly true for the participation in the mutual data exchange by organisations within the Soviet Union.

The flow of information and observational data from USSpaceCom (via NASA JSC and GSFC), from the Soviet authorities (IKI, MCC, and MoD), from the German research establishment FGAN, and from RAE in the UK, combined with the lifetime prediction estimates from CNES/Toulouse and CNUCE/Pisa, for the first time enabled ESA to closely monitor the decay of a large size object, and perform near real-time re-entry prediction computations.

The re-entry forecasts which were produced by ESA/ESOC and distributed to national points of contact within the USA, the USSR, and ESA Member States (including Canada), were of good accuracy, and closely matching results from the US and USSR until shortly ($t - 12h$) before the final decay. Thereafter, due to difficulties in the interpretation of the Soviet orbit determination results, and due to larger time lags in the acquisition of the USSpaceCom TLE data, a real-time determination of the re-entry time and location could not be provided by ESOC with satisfactory accuracy[1].

After the identification of systematic differences between the TLEs of USSpaceCom and the ESOC derived Kepler states from the Soviet orbit determinations (which only showed below 200 km altitude), a separation of the data and a separate estimation of the drag coefficient provided an accurate re-construction of the impact trace (for both data sources) by the time when the complete orbit state histories reached ESOC (see Fig.6 and Tab.3,4).

Acknowledgements

The author gratefully acknowledges the efficient support during the Salyut-7/Kosmos-1686 re-entry campaign by the following national space agencies, and research institutes within the USA, the USSR, and the ESA Member States: NASA (JSC and GSFC), IKI (the Institute for Cosmic Research), the USSR Ministry of Defence, TSUP (USSR Mission Control), FGAN (the Research Establish-

[1] both of these problems have been discussed with the parties involved; procedures for their resolution have been identified and are currently under investigation

ment for Applied Science, FRG), and RAE (the Royal Aerospace Establishment, UK).

ESA also appreciates the re-entry prediction information provided by CNUCE/CNR (Pisa), and by CNES/CST (Toulouse).

Special thanks also goes to my colleagues Dr. W.Flury, Dr. G.Janin, and R.Jehn for their support during the Salyut-7/Kosmos-1686 re-entry campaign.

References

1. K. Aksnes
Short-Periodic and Long-Periodic Perturbations of a Spherical Satellite due to Direct Solar Radiation
Celestial Mech. 13 (1976), p.89-104

2. L. Blitzer
Nodal Period of an Earth Satellite
AIAA Journal, Vol.2, Aug.1964, p.1459-1460

3. G.E. Cook
Basic Theory for PROD, a Program for Computing the Development of Satellite Orbits
Celestial Mechanics 7(1972), p.301-314

4. G. Janin, M. Bello-Mora
A Flexible Tool for the Calculation of Orbits in the Solar System, **Adv. of Space Res.**, Vol.10, No.3-4, 1990, p.327-330

5. W.M. Kaula
Theory of Satellite Geodesy
Blaisdel Publ. Comp., Waltham, Mass.-Toronto-London, 1966

6. H. Klinkrad
Analytical Prediction of Close-Earth Satellite Orbits Using a Realistic Drag Force Model (in German)
Ph.D Dissertation, Techn. Univ. Braunschweig, Mar.1984

7. J.J.F. Liu, R.L. Alford
A Semi-Analytic Theory for the Motion of a Close-Earth Artificial Satellite with Drag
AIAA Paper, No.79-0123, 17th Aerospace Sciences Meeting, New Orleans/La., Jan.15-17, 1979

8. R. Mugellesi
The SOLMAG Forecast System for Solar and Geomagnetic Activity
ESOC/OAD Working Paper No.416, ESA/ESOC, Mar.1990

9. N. Longdon (Editor)
Re-Entry of Space Debris
ESA SP-246, Proceedings of an ESA Workshop held at ESOC, Darmstadt/FRG, 24-25 Sep.1985